

ECHOGEN: GENERATING VISUAL ECHOES IN ANY SCENE VIA FEED-FORWARD SUBJECT-DRIVEN AUTO-REGRESSIVE MODEL

Anonymous authors

Paper under double-blind review

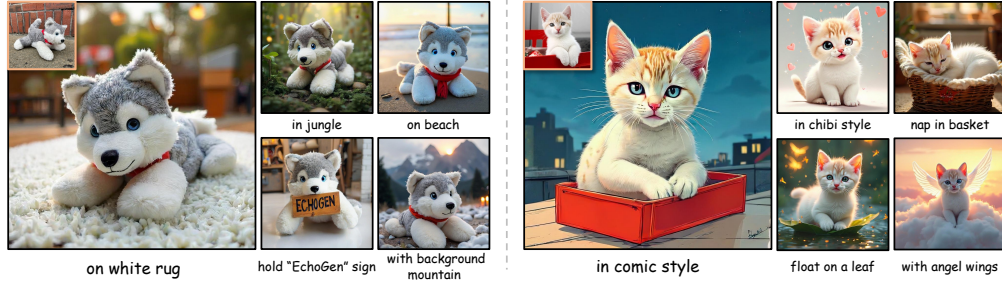


Figure 1: **Feed-forward subject-driven generation by EchoGen.** By employing a visual autoregressive paradigm, EchoGen achieves both high-quality image synthesis with lower latency, preserving intricate subject identity with exceptional efficiency.

ABSTRACT

Subject-driven generation is a critical task in creative AI; yet current state-of-the-art methods present a stark trade-off. They either rely on computationally expensive, per-subject fine-tuning, sacrificing efficiency and zero-shot capability, or employ feed-forward architectures built on diffusion models, which are inherently plagued by slow inference speeds. Visual Auto-Regressive (VAR) models are renowned for their rapid sampling speeds and strong generative quality, making them an ideal yet underexplored foundation for resolving this tension. To bridge this gap, we introduce **EchoGen**, a pioneering framework that empowers VAR models with subject-driven generation capabilities. The core design of EchoGen is an effective dual-path injection strategy that disentangles a subject’s high-level semantic identity from its low-level fine-grained details, enabling enhanced controllability and fidelity. We employ a semantic encoder to extract the subject’s abstract identity, which is injected through decoupled cross-attention to guide the overall composition. Concurrently, a content encoder captures intricate visual details, which are integrated via a multi-modal attention mechanism to ensure high-fidelity texture and structural preservation. To the best of our knowledge, EchoGen is the first feed-forward subject-driven framework built upon VAR models. Both quantitative and qualitative results substantiate our design, demonstrating that EchoGen achieves subject fidelity and image quality comparable to state-of-the-art diffusion-based methods with significantly lower sampling latency.

1 INTRODUCTION

The rapid evolution of text-to-image synthesis models (Saharia et al., 2022; Rombach et al., 2022; Batifol et al., 2025; Esser et al., 2024) has catalyzed a variety of novel applications (Zhang et al., 2023), among which subject-driven generation stands out as an important task. This task aims to accurately depict a specified subject within diverse, user-defined scenes described through text prompts, while rigorously upholding the subject’s core identity. The early approaches (Ruiz et al., 2023; Gal et al., 2022; Kumari et al., 2023) introduced a test-time fine-tuning paradigm that optimizes a large pretrained model using a few images for each new subject. Although effective in preserving identity to some extent, this per-subject optimization process is computationally expen-

054 sive, demanding at least hundreds of training iterations and substantial GPU resources, ultimately
 055 resulting in a distinct model checkpoint for each subject. These limitations significantly hinder the
 056 practicality and scalability of the test-time fine-tuning paradigm in real-world applications.
 057

058 To improve efficiency and practicality, a new class of feed-forward approaches has recently
 059 emerged (Li et al., 2023; Pan et al., 2024; Ye et al., 2023; Tan et al., 2025; Shin et al., 2025)
 060 based on diffusion models (Rombach et al., 2022; Podell et al., 2024; Batifol et al., 2025). In-
 061 stead of fine-tuning on a small set of images for each new subject, feed-forward approaches perform
 062 a single, large-scale supervised fine-tuning on a vast dataset composed of triplets (text, reference
 063 image, target image). The model is trained to learn a generalizable mapping from a subject image
 064 to the snapshot version in the specified scene. The single process of pretraining enables zero-shot
 065 generation at inference time—a novel subject can be synthesized immediately without any subject-
 066 specific fine-tuning, significantly reducing the initial setup cost and decreasing generation latency
 067 by eliminating the need for test-time optimization. Nevertheless, these methods still inherit the
 068 computational demands of the underlying diffusion models due to the iterative denoising process.
 069

070 Inspired by autoregressive generation in language models (Radford et al., 2018; Achiam et al.,
 071 2023), autoregressive visual generation (Esser et al., 2021; Ramesh et al., 2021; Sun et al., 2024)
 072 has emerged as a compelling alternative to diffusion models. Unlike diffusion’s iterative denoising,
 073 autoregressive models synthesize content sequentially, token by token. This paradigm is further
 074 advanced by the Visual Autoregressive (VAR) model (Tian et al., 2024; Han et al., 2025), which
 075 employs a coarse-to-fine *next-scale* generation strategy instead of traditional *next-token* generation.
 076 It first generates tokens for the global composition and then renders fine-grained details, capturing a
 077 complete hierarchical representation from structure to texture. The novel paradigm allows VAR to
 078 achieve superior performance compared to traditional autoregressive models, outperforming top-tier
 079 diffusion models while offering faster inference speed. Despite the inherent suitability of the autore-
 080 gressive paradigm for fine-grained conditioning, its potential for controllable generation, especially
 081 in the feed-forward, subject-driven context, remains largely untapped compared to the wealth of
 082 research on diffusion-based methods. This critical gap severely limits the practical applicability of
 083 VAR models, hindering their adoption in real-world scenarios where subject control is paramount.
 084

085 In this work, we aim to bridge this gap by leveraging the inherent advantages of VAR to build an
 086 effective, scalable, and highly controllable system for subject-driven image synthesis. We propose
 087 *EchoGen*, the first efficient **feed-forward** autoregressive framework that generates faithful visual
 088 renditions of a given subject in arbitrary scenes. At the core of EchoGen is a *dual-path* injection
 089 mechanism that disentangles semantic features from fine-grained details. We inject high-level fine-
 090 grained semantic features extracted by a semantic encoder based on the pretrained vision foundation
 091 model (DINOv2 (Oquab et al., 2024)) into the decoupled cross-attention layers (Kumari et al., 2023)
 092 to bring structural and stylistic coherence while avoiding drift in prompt following. To enable global
 093 semantic conditioning, we prepend the global semantic embedding extracted from DINOv2 as a
 094 prefix and subsequently infuse it via Adaptive LayerNorm, thereby steering the overall semantic
 095 generation. However, generating with semantic features alone often misses low-level details. To
 096 complement these features, a second pathway employs a pretrained content encoder (FLUX.1-dev
 097 VAE (Batifol et al., 2025)) to extract fine-grained image features, which are incorporated via a
 098 multi-modal attention module, ensuring faithful reconstruction of local textures and details. To
 099 preserve the generative capabilities of the pretrained VAR model, we adopt a parameter-efficient
 100 fine-tuning strategy that freezes the backbone and only updates key components within the subject
 101 injection modules. Extensive quantitative and qualitative evaluations on DreamBench (Ruiz et al.,
 102 2023) benchmark and human evaluation demonstrate that EchoGen achieves subject fidelity, text
 103 alignment, and image quality comparable to and even exceeding state-of-the-art diffusion-based
 104 methods, while exhibiting lower sampling latency.
 105

106 Our principal contributions can be summarized as follows:
 107

- 108 • We introduce EchoGen, the first feed-forward, efficient, subject-driven generation frame-
 109 work built upon a visual autoregressive model. This establishes a compelling new paradigm
 110 for controllable subject-driven synthesis beyond the dominant diffusion-based approaches.
 111
- 112 • We propose a novel dual-path injection strategy that disentangles the identity of a sub-
 113 ject into high-level semantics and fine-grained details. By injecting these features through
 114 separate pathways within a parameter-efficiently tuned model, EchoGen achieves faithful
 115 subject representation across diverse scenes.
 116

108 • Extensive experiments demonstrate that EchoGen achieves subject fidelity, text alignment,
 109 and image quality that are competitive with or superior to state-of-the-art diffusion-based
 110 methods with much faster inference speed.
 111

112 **2 RELATED WORKS**

113 **2.1 AUTOREGRESSIVE IMAGE GENERATION**

114 Unlike diffusion-based methods that synthesize images via iterative denoising, the autoregressive
 115 paradigm models image distributions by sequentially predicting visual tokens conditioned on the
 116 preceding context. This approach evolves from inefficient and low quality early pixel-level meth-
 117 ods (Van den Oord et al., 2016; Salimans et al., 2017) to a dominant two-stage framework that
 118 first compresses images into discrete tokens and then models their distribution utilizing Trans-
 119 former (Esser et al., 2021). This paradigm substantially improves generation fidelity and efficiency,
 120 underpinning advances in text-to-image synthesis (Ramesh et al., 2021; Yu et al., 2022b) and con-
 121 trollable generation (Li et al., 2025). Subsequent work further refines it by improving image tok-
 122 enizers (Yu et al., 2022a; Mentzer et al., 2024), exploring continuous representations with diffusion
 123 modeling (Li et al., 2024a; Fan et al., 2025), or adapting large language models for visual gener-
 124 ation (Sun et al., 2024; Wu et al., 2024). To mitigate structural degradation induced by the fixed
 125 raster-scan order, Visual Autoregressive (VAR) models (Tian et al., 2024) introduce a hierarchical
 126 coarse-to-fine strategy that progressively refines fine-grained details by next-scale prediction. The
 127 following version Infinity (Han et al., 2025) extends the VAR model to text-to-image generation,
 128 achieving superior quality with significantly lower sampling latency than diffusion models. While
 129 existing works extend VAR to controllable generation (Yao et al., 2024; Li et al., 2024b; Chung
 130 et al., 2025), feed-forward subject-driven personalization remains underexplored, limiting the prac-
 131 tical applicability of the VAR framework.

132 **2.2 SUBJECT-DRIVEN IMAGE GENERATION**

133 **Test-time fine-tuning methods.** Diffusion models (Ho et al., 2020; Rombach et al., 2022) have
 134 achieved remarkable success in high-fidelity text-to-image (T2I) synthesis (Podell et al., 2024; Esser
 135 et al., 2024; Batifol et al., 2025). For subject-driven tasks, relying solely on text prompts is often
 136 insufficient to preserve the defining characteristics of specific subjects. To address this, pioneering
 137 methods (Gal et al., 2022; Ruiz et al., 2023; Kumari et al., 2023) introduce customization by fine-
 138 tuning on a small set of reference images for each target subject. While these approaches can
 139 capture intricate details and deliver high fidelity to some extent, their dependence on per-subject
 140 optimization remains time-consuming and computationally demanding, which limits practical use.
 141

142 **Feed-forward subject-driven approaches.** To overcome the efficiency limitations of per-subject
 143 optimization, feed-forward methods have been developed (Wei et al., 2023; Zeng et al., 2024; Patel
 144 et al., 2024; Ma et al., 2024; Wang et al., 2025). These models are trained once to condition on
 145 subject features from vision encoders, enabling fast, zero-shot synthesis for novel subjects. Early
 146 works such as BLIP-Diffusion (Li et al., 2023) jointly fine-tune the denoising network with multi-
 147 modal alignment modules while suffering from inadequate fidelity and image quality. To mitigate
 148 the high computational cost of full model tuning, parameter-efficient strategies (Pan et al., 2024; Ye
 149 et al., 2023; Tan et al., 2025; Zhang et al., 2025; Wu et al., 2025) incorporate lightweight modules
 150 such as LoRA (Hu et al., 2022) or adapters. These modules inject reference features into the diffu-
 151 sion transformer, typically via attention mechanisms, while keeping most pretrained weights frozen.
 152 However, since these methods all rely on diffusion backbones, they inherit the substantial inference
 153 latency of the iterative denoising process, which constrains their practical deployment.

154 **3 PRELIMINARY OF VISUAL AUTOREGRESSIVE MODELING**

155 Autoregressive models (Esser et al., 2021) reframe image synthesis as a sequential token predic-
 156 tion, under the *next-token* prediction. The image is first tokenized into a discrete feature map us-
 157 ing a visual tokenizer \mathcal{E} and then flattened into a one-dimensional sequence, typically following
 158 the raster scan order. The model is then trained to predict each token x_i given the preceding to-
 159 kens (x_1, \dots, x_{i-1}) and the condition c , factorizing the sequence distribution as $p(x_1, \dots, x_N | c) =$
 160 $\prod_{i=1}^N p(x_i | x_1, \dots, x_{i-1}, c)$. However, the vanilla next-token paradigm with fixed raster order in-
 161 duces structural degradation and insufficient modeling.

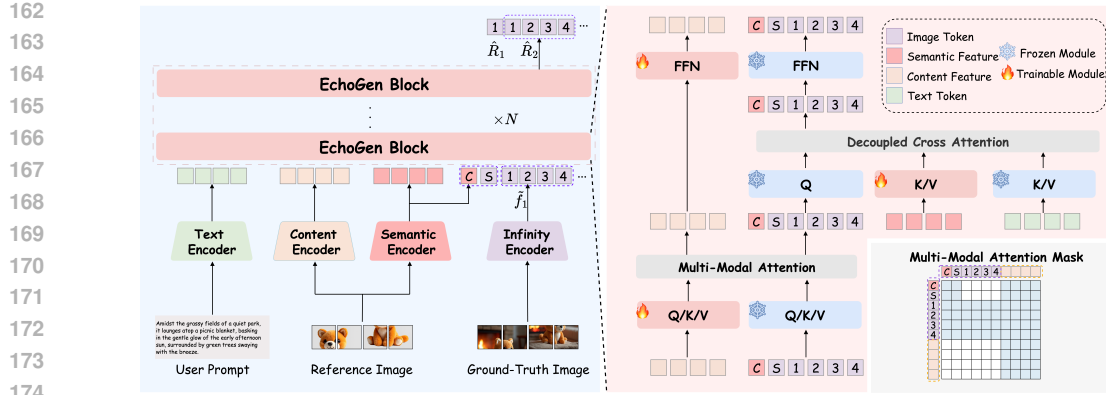


Figure 2: **Overview of the EchoGen architecture.** The left panel illustrates the overall model framework with dual-path subject injection, while the right panel provides a detailed schematic of the EchoGen block with a carefully designed attention mask applied in the Multi-Modal Attention module to avoid feature leakage. C denotes the global semantic token extracted from the semantic encoder, which is prepended to the input sequence. S represents the start token for the first-scale generation. Adaptive Layer Normalization modules in the EchoGen blocks are omitted for clarity.

Visual autoregressive modeling (Tian et al., 2024) addresses the above issues by shifting the prediction paradigm from *next-token* to *next-scale*: instead of predicting one token at a time, it predicts entire token maps at *progressively increasing resolutions*. The visual encoder \mathcal{E} first maps an image I to latent F , and then produces K multi-scale token maps (r_1, \dots, r_K) with increasing resolutions $h_k \times w_k$ by applying a residual vector quantizer. A GPT-style Transformer begins from the generation of the 1×1 map r_1 and autoregressively predicts each subsequent scale given prior scales and condition c , achieving generation from global structure to fine details, which is formulated as:

$$p(r_1, \dots, r_K | c) = \prod_{k=1}^K p(r_k | r_1, \dots, r_{k-1}, c). \quad (1)$$

This scale-wise coarse-to-fine paradigm is well suited for scalable text-to-image generation. The text-to-image generation model Infinity (Han et al., 2025) leverages bitwise quantization to expand the vocabulary size under the next-scale paradigm, reporting state-of-the-art performance with reduced sampling latency compared to diffusion baselines. In this paper, to bypass the cumbersome per-subject fine-tuning and the heavy computational cost during inference, we propose a novel feed-forward framework based on VAR models, featuring a single parameter-efficient fine-tuning phase.

4 ECHOGEN

4.1 OVERALL FRAMEWORK

We are seeking a novel feed-forward framework for subject-driven generation built upon Infinity, based on the proposed **EchoGen** block with effective dual-path subject information injection, in which a content encoder and a semantic encoder cooperate to provide comprehensive subject features from both sides of a coin. The overview of the EchoGen architecture and its basic block is illustrated in Figure 2. Before subject injection, to ensure robustness against background noise that may interfere with subject injection, a pipeline based on the multi-modality model Qwen2.5-VL (Bai et al., 2025) and the open segmentation model GroundingDINO (Liu et al., 2024) is carefully designed to segment the subject from complex scenes. Given the segmented subject image, our EchoGen model is trained using a parameter-efficient methodology that freezes the pretrained backbone while fine-tuning only newly introduced attention modules. During inference, we apply flexible subject-text classifier-free guidance for explicit control over the trade-off between subject fidelity and textual alignment, enabling versatile and controllable generation.

4.2 DUAL-PATH SUBJECT INJECTION

Semantic feature injection for identity preservation. The semantic feature, which captures abstract characteristics, provides a representation that is critical for avoiding the identity drift com-

mon in subject-driven generative models. Following this principle, we introduce a bifurcated injection strategy that targets both the fine-grained and global levels of the generative process. For fine-grained conditioning, we employ the pretrained DINOv2 vision encoder to extract patch-level semantic embeddings. These embeddings are synergistically integrated with the original textual conditioning via a decoupled cross-attention mechanism (Kumari et al., 2023). Our decoupled cross-attention mechanism operates on query features \mathcal{Z} , conditioning them on both the text embedding c_t and the fine-grained semantic features c_s , formulated as follows:

$$\begin{aligned} \mathcal{Q} &= \mathcal{Z} W^q, \mathcal{K} = \text{concat}(c_s W_s^k, c_t W_t^k), \mathcal{V} = \text{concat}(c_s W_s^v, c_t W_t^v), \\ \mathcal{Z}' &= \text{Attention}(\mathcal{Q}, \mathcal{K}, \mathcal{V}) = \text{Softmax}\left(\mathcal{Q}\mathcal{K}^\top/\sqrt{d}\right)\mathcal{V}, \end{aligned} \quad (2)$$

where W^q is the query projector, (W_t^k, W_t^v) and (W_s^k, W_s^v) are two distinct sets of (k, v) projectors to embed text prompting c_t and semantic injection c_s , respectively. The resulting key and value pairs for each condition are concatenated to form the final context vectors \mathcal{K} and \mathcal{V} . We keep the projectors for text prompting (W_t^k, W_t^v) and the query projector W^q frozen while exclusively optimizing the key and value projectors (W_s^k, W_s^v) that map the semantic features of the reference images, enabling an alignment mapping from the semantic visual space to the generator’s latent space without perturbing the pretrained knowledge.

Moreover, we prepend the DINOv2 global semantic token C to the input sequence to impose holistic semantic guidance. At the same time, this global token also serves as a condition for the Adaptive Layer Normalization (AdaLN) layer in the proposed EchoGen block, following (Han et al., 2025). The infusion of fine-grained and global semantics ensures comprehensive semantic-informed generation, promoting fine-grained fidelity and global structural coherence.

Content feature injection for detail preservation. While the semantic embeddings provide a robust identity preservation, their high abstraction leads to generation with insufficient subject details. To achieve high fidelity of the subject’s content, we complement it with a content feature infusion mechanism. To be specific, EchoGen employs the FLUX.1-dev VAE to extract low-level content features c_c , which are then integrated via the multi-modal attention. The generation process is then steered by a carefully designed attention operation: generated tokens have unobstructed access to the reference tokens, allowing them to distill fine-grained visual cues on demand; conversely, a causal mask renders the reference tokens oblivious to the generated sequence, which is a critical constraint for ensuring the autoregressive sampling trajectory. This masking schema is precisely demonstrated in the lower-right inset of Figure 2. Specifically, given the generated token sequence \mathcal{Z} and the detailed content condition c_c , the multi-modal attention utilizes separate linear projections (W^q, W^k, W^v) for \mathcal{Z} and (W_c^q, W_c^k, W_c^v) for the condition c_c , with the applied attention mask Mask, and then calculate the generated sequence \mathcal{Z}' and condition c_c' via:

$$\begin{aligned} \mathcal{Q} &= \text{concat}(\mathcal{Z} W^q, c_c W_c^q), \mathcal{K} = \text{concat}(\mathcal{Z} W^k, c_c W_c^k), \mathcal{V} = \text{concat}(\mathcal{Z} W^v, c_c W_c^v), \\ \mathcal{Z}', c_c' &= \text{Attention}(\mathcal{Q}, \mathcal{K}, \mathcal{V}, \text{Mask}) = \text{Softmax}\left(\text{Mask}\left(\mathcal{Q}\mathcal{K}^\top/\sqrt{d}\right)\right)\mathcal{V}. \end{aligned} \quad (3)$$

The pathways for the generated token sequence remain frozen, while exclusively parallel attention projectors (W_c^q, W_c^k, W_c^v) and FFN modules for processing content features are optimized.

Through this dual-path subject injection strategy, our model faithfully preserves the salient visual characteristics of the reference image while simultaneously maintaining a strong adherence to the provided text instructions.

4.3 SUBJECT SEGMENTATION

A common challenge in real-world scenarios is that user-provided reference images comprised of the subject of interest within visually complex backgrounds may harm the performance of subject injection. To mitigate this issue, we employ a subject segmentation pre-processing pipeline, illustrated in Figure 3. First, the Qwen2.5-VL (Bai et al., 2025) vision-language model identifies the subject’s semantic identity, producing a descriptive text prompt. This prompt

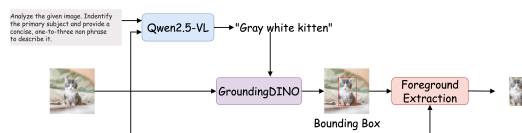


Figure 3: The pipeline of subject segmentation.

270 is then used to condition the GroundingDINO (Liu et al., 2024) model for precise subject local-
 271 ization and bounding box generation. The foreground region is subsequently cropped according to
 272 this bounding box, while the surrounding unrelated regions are explicitly discarded and replaced
 273 with a uniform white background. This process ensures that subsequent feature injection operates
 274 attentively on the isolated representation of the referred subject.

275 4.4 SAMPLING WITH SUBJECT-TEXT CLASSIFIER-FREE GUIDANCE

276 Classifier-Free Guidance (CFG) (Ho & Salimans, 2021) has become a cornerstone technique for
 277 enhancing conditional control in generative models, especially in diffusion models. Its core principle
 278 is to amplify the conditional signal by extrapolating from an unconditional prediction towards a
 279 conditional one, thereby improving condition following at the cost of some diversity. Recently,
 280 many autoregressive models (Chang et al., 2023; Tian et al., 2024) have also incorporated CFG into
 281 their frameworks. In this work, we further enhance the influence of the text embedding c_t and the
 282 subject condition c_s, c_c within the CFG scheme for subject-driven generation. During training, we
 283 independently replace the text condition c_t with an unconditional token \emptyset_t and the image condition
 284 c_s, c_c with unconditional embeddings \emptyset_s, \emptyset_c , each with a probability of 10%. During inference,
 285 assuming the independence between the text condition c_t and the image condition c_s, c_c , we compute
 286 the final logits predicted by EchoGen via a flexible guidance rule that integrates both controls:

$$287 \hat{l} = l(\emptyset_t, \emptyset_s, \emptyset_c) + \gamma_t \times (l(c_t, \emptyset_s, \emptyset_c) - l(\emptyset_t, \emptyset_s, \emptyset_c)) + \gamma_I \times (l(c_t, c_s, c_c) - l(c_t, \emptyset_s, \emptyset_c)), \quad (4)$$

288 where l denotes the Transformer output logits, and γ_t together with γ_I are hyperparameters that
 289 govern the guidance scales. This dynamic text-subject guidance not only strengthens the influence of
 290 text embeddings and image prompts, thereby improving generation performance, but also provides
 291 a flexible mechanism to balance text alignment with the reference preservation.

294 5 EXPERIMENT

295 5.1 SETUP

296 **Datasets.** We conduct experiments on the Subjects200K dataset (Tan et al., 2025), a substantial
 297 collection comprising about 256,000 triplets of text prompts, reference images, and target images.
 298 The corpora were generated using GPT-4o and FLUX.1-dev, and with image resolutions larger than
 299 500×500. For EchoGen-0.1B training, both the reference and target images are resized and center-
 300 cropped to 256×256. To enable high-resolution generation for EchoGen-2B training, we avoid
 301 direct interpolation, which may introduce undesirable artifacts; instead, we upscale the images to
 302 1024×1024 using the PiSA-SR super-resolution model (Sun et al., 2025).

303 **Training details.** Our training protocol largely follows Infinity (Han et al., 2025). We train EchoGen
 304 for 400k iterations, utilizing the AdamW (Loshchilov & Hutter, 2017) optimizer with a global batch
 305 size of 128, setting the base learning rate as 3×10^{-5} and the momentum parameters $(\beta_1, \beta_2) =$
 306 $(0.9, 0.97)$. To stabilize fine-tuning, we apply a reduced learning rate of 3×10^{-6} to the multi-modal
 307 attention parameters. More training details can be found in the appendix 7.3.1.

308 **Evaluation.** Following prior works (Ruiz et al., 2023; Li et al., 2023), we evaluate our approach
 309 in terms of subject fidelity and text alignment on the DreamBench benchmark (Ruiz et al., 2023).
 310 Subject fidelity is measured by the cosine similarity between the generated and reference images
 311 using both CLIP (Radford et al., 2021) image embeddings (CLIP-I) and DINO (Zhang et al., 2022)
 312 features (DINO). Text alignment is assessed via the CLIP cosine similarity between the generated
 313 image and its corresponding input prompt (CLIP-T). DreamBench, comprising real-world images
 314 with prompt annotations, includes 30 unique subjects, each paired with 25 distinct prompts. Follow-
 315 ing the standard protocol, we generate four images for each prompt-subject pair, yielding a total of
 316 3,000 images for evaluation.

317 5.2 MAIN RESULTS

318 We compare EchoGen with three categories of prior works: (1) test-time fine-tuning methods that
 319 require per-subject optimization; (2) unified generation models with large-scale pre-training; and (3)
 320 feed-forward approaches that share the same paradigm as ours and constitute our most baselines.

321 **Quantitative results.** We benchmark EchoGen performance against contemporary subject-driven
 322 diffusion-based methods in the DreamBench dataset (Ruiz et al., 2023), with quantitative results

Method	Base Model	DINO \uparrow	CLIP-I \uparrow	CLIP-T \uparrow	Latency \downarrow
<i>Test-time Fine-tuning</i>					
Textual-Inversion (Gal et al., 2022)	SD-v1.5	0.569	0.780	0.255	50min
DreamBooth (Ruiz et al., 2023)	SD-v1.5	0.668	0.803	0.305	15min
BLIP-Diffusion (Li et al., 2023)	SD-v1.5	0.670	0.805	0.302	-
AR-Booth (Chung et al., 2025)	Infinity-2B	0.750	0.808	0.269	2.8h
<i>Unified Generation</i>					
OmniGen (Xiao et al., 2025)	OmniGen	0.693	0.801	0.315	93.4s
<i>Feed-Forward</i>					
ELITE (Wei et al., 2023)	SD-v1.4	0.621	0.771	0.293	11.0s
Re-Imagen (Chen et al., 2023)	Imagen	0.600	0.740	0.270	-
BLIP-Diffusion (Li et al., 2023)	SD-v1.5	0.594	0.779	0.300	-
λ -Eclipse (Patel et al., 2024)	Kan-v2.2	0.613	0.783	0.307	-
BootPIG (Purushwalkam et al., 2024)	SD-v2.1	0.674	0.797	0.311	-
MS-Diffusion (Wang et al., 2025)	SDXL	0.671	0.792	0.321	39.6s
IP-Adapter (Ye et al., 2023)	SDXL	0.613	0.810	0.292	16.9s
IP-Adapter (Ye et al., 2023)	FLUX.1-dev	0.561	0.725	0.351	-
OminiControl (Tan et al., 2025)	FLUX.1-dev	0.684	0.799	0.312	27.5s
EasyControl (Zhang et al., 2025)	FLUX.1-dev	0.652	0.789	0.325	47.6s
EchoGen-0.1B	Infinity-0.1B	0.675	0.806	0.321	0.5s
EchoGen-2B	Infinity-2B	0.755	0.837	0.324	5.2s

Table 1: **Quantitative comparisons on DreamBench (Ruiz et al., 2023)**. We highlight the best, second-best, and third-best values for each metric. The results indicate that EchoGen attains performance on par with diffusion-based approaches while delivering substantially faster sampling.

Method	Subject Fidelity \uparrow	Text Alignment \uparrow	Photorealism \uparrow
OmniGen (Xiao et al., 2025)	0.15	0.13	0.09
IP-adapter (Ye et al., 2023)	0.21	0.05	0.14
OminiControl (Tan et al., 2025)	0.12	0.21	0.15
EasyControl (Zhang et al., 2025)	0.15	0.31	0.28
EchoGen-2B	0.37	0.30	0.34

Table 2: **Human evaluation**. We compare our method with previous approaches based on three aspects: text alignment, subject fidelity, and photorealism.

summarized in Table 1. EchoGen achieves performance that superior to leading diffusion-based approaches in the core metrics of subject fidelity and text alignment, and demonstrates balanced performance across evaluation axes. In contrast, several baselines, such as IP-Adapter (Ye et al., 2023) exhibit significant weaknesses in specific metrics. Furthermore, the adoption of the visual autoregressive paradigm provides a clear efficiency advantage: EchoGen’s inference latency for a 1024×1024 image is under 6 seconds, representing a significant acceleration over the more than 10 seconds required by its diffusion-based counterparts. Overall, these results indicate that EchoGen combines strong generative quality with markedly improved efficiency, offering a competitive alternative for subject-driven synthesis.

Qualitative results. Figure 4 presents a rigorous qualitative comparison with prominent diffusion-based frameworks, revealing substantial advantages of our model in both subject fidelity and prompt correspondence. EchoGen exhibits the ability to render high-fidelity details, such as the precise reconstruction of the teapot spout and the nuanced texture of the sloth plushie, and we attribute this capability to our dual-path semantic-content feature injection design. In contrast, baselines including IP-Adapter (Ye et al., 2023) and OminiControl (Tan et al., 2025) exhibit characteristic failure cases, corroborating EchoGen’s robustness. EchoGen also demonstrates more consistent compliance with

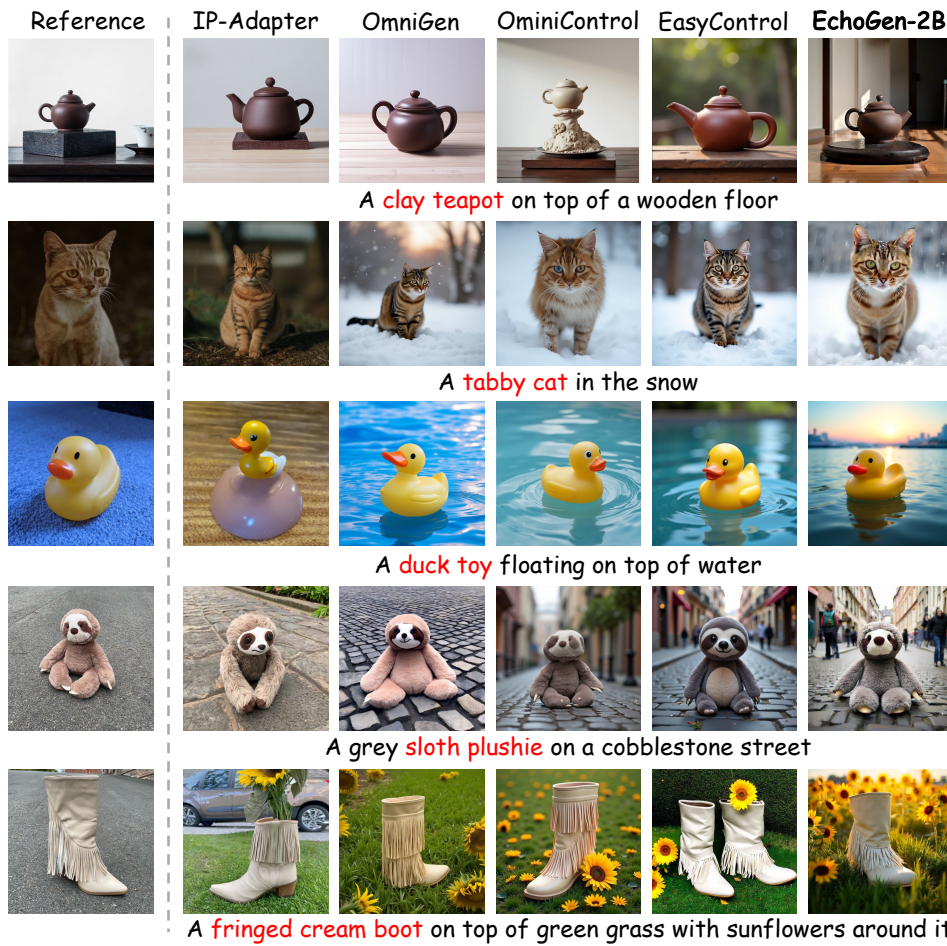


Figure 4: **Qualitative comparison with diffusion-based methods on DreamBench (Ruiz et al., 2023).** For a fair comparison, we adopt the default sampling settings for all baseline models.

textual prompts, avoiding the language deviations observed in the generations of the duck toy and cat instances by IP-Adapter.

Human evaluation. To assess the perceptual quality of EchoGen, we conduct a human evaluation study against strong baselines that span multiple categories of subject-driven methods. We focus on three criteria: text alignment, subject fidelity, and photorealism. The images are generated conditioned on the reference images and prompts sampled from DreamBench (Ruiz et al., 2023) and DreamBench++ (Peng et al., 2024) benchmarks **without any cherry-picking**, and for each criterion, participants select their preferred generated image among the outputs from five methods. We collect 450 responses from 25 participants, **all with expertise in generative models**, and report preference ratios in Table 2. The results show that EchoGen is preferred for subject fidelity and photorealism, surpassing all the diffusion-based contemporary baselines on these criteria. For text alignment, EchoGen performs on par with EasyControl (Zhang et al., 2025) and exhibits a clear advantage over the other compared methods.

Sampling Latency Analysis. We conduct a thorough analysis to evaluate the performance-latency trade-offs across all methods. Specifically, we evaluate diffusion-based methods with varying numbers of denoising steps and report their performance versus sampling latency in Figure 5. For the diffusion baselines, increasing the number of denoising steps improves subject fidelity (as measured by DINO, CLIP-I scores) up to a saturation point. In contrast, the text alignment (CLIP-T) score converges much earlier. Our model consistently offers a better trade-off, achieving superior performance with significantly lower sampling latency than the diffusion-based baselines. This confirms the inherent efficiency and effectiveness of our approach.

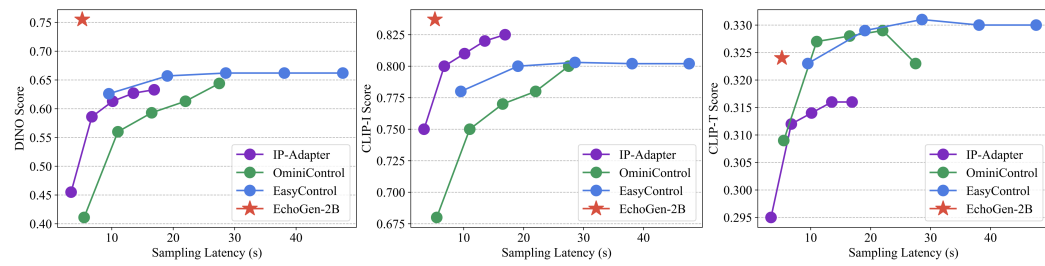


Figure 5: Performance v.s. sampling latency comparison among our EchoGen and baselines.

Enc.	DINO↑	CLIP-I↑	CLIP-T↑
SigLIP-2	0.438	0.720	0.320
FLUX.1-dev	0.433	0.706	0.320
DINOv2	0.670	0.798	0.322

Table 4: Significance of fine-grained semantic injection. “Enc.” denotes the encoder type.

The detailed component-wise sampling latency of our EchoGen framework is provided in Table 3. The results confirm that the framework’s overall efficiency is not limited by auxiliary components such as Grounding-DINO. EchoGen maintains a significant speed advantage over diffusion-based methods, even with the inclusion of the optional Qwen2.5-VL model. Although this model is employed during training to automate subject identification for the GroundingDINO segmentation model, it is not required during inference. Instead, users can provide a descriptive text prompt (akin to the DreamBench format) for specifying the subject.

5.3 ABLATION STUDIES

We conduct a series of ablation studies to verify the effect of each component in EchoGen. Owing to computational constraints, all experiments are performed on EchoGen-0.1B with the same training settings to ensure fair ablation studies.

Significance of fine-grained semantic information injection. Fine-grained semantic conditional information is critical as it provides guidance for establishing the structure, enabling the model to synthesize stylistically and structurally coherent features consistent with the subject. Conversely, we argue that overly coarse-grained semantic features may fail to provide sufficient guidance for generating visually consistent echoes. To validate the importance of incorporating fine-grained semantic information, we conducted an ablation study with three distinct feature types independently injected via cross-attention: (1) coarse-grained semantic identity from SigLIP-2 (Tschannen et al., 2025), (2) fine-grained semantic features from DINOv2 and (3) FLUX.1-dev VAE features, which lack enough semantic information. Table 4 demonstrates that the fine-grained semantic DINOv2 features are the most suitable to represent the echo information in this task, as evidenced by all criteria. The failure of the SigLIP-2 and FLUX.1-dev VAE features can be attributed to their respective limitations: the former relies on features that are too coarse to guide subject generation, while the latter lacks semantic information.

Incorporating the global semantic information. To provide stronger guidance when constructing the global structure in the generation process, we prefix the global semantic C token extracted by the DINOv2 semantic encoder and incorporate this token into the model via Adaptive LayerNorm. As demonstrated in Table 5, compared with solely relying on injecting fine-grained semantic features via cross-attention, the introduction of the global semantic token yields a substantial performance gain in consistency of subject characteristics, validating the effectiveness of incorporating global semantic information.

Exp.	DINO↑	CLIP-I↑	CLIP-T↑
w/o prefix	0.632	0.788	0.328
w prefix	0.670	0.798	0.322

Table 5: Ablation study on incorporating the global semantic features of reference images.

Model Component	Sampling Latency (s)
Grounding-DINO	0.24
Semantic encoder	0.008
Content encoder	0.025
Infinity generator	4.95
Qwen2.5-VL(Optional)	1.13
EchoGen (w/o Qwen2.5-VL)	5.22
EchoGen (w/ Qwen2.5-VL)	6.35

Table 3: Per-component sampling latency measured on a single H20 GPU.

can provide a descriptive text prompt (akin to the DreamBench format) for specifying the subject.

486
487 Distinct semantic feature injection strate-
 488 **gies.** We explore the most effective method to
 489 guide the synthesis process conditioned on the
 490 semantic features of reference images. Table 6
 491 presents an analysis comparing two distinct fea-
 492 ture injection modules: multi-modal attention
 493 and cross-attention. Our results indicate that
 494 while the multi-modal module achieves slightly
 495 better alignment with text prompts, the cross-atten-
 496 tion mechanism yields significantly superior sub-
 497 ject fidelity, as evidenced by a notably higher DINO
 498 score. Based on this, we opted to utilize
 499 cross-attention for injecting the semantic features in all
 500 subsequent experiments, rather than the
 501 multi-modal attention.
 502

503 **504 Enhancing subject fidelity with detailed con-
 505 tent features.** Considering the absence of lo-
 506 cal details in the semantic features of the refer-
 507 ence images, we incorporate a secondary path-
 508 way that injects localized content features of
 509 the subject. These features, extracted by the
 510 FLUX.1-dev VAE, are used to guide the synthe-
 511 sis of the fine-grained local details of the sub-
 512 ject. The ablation study detailed in Table 7 de-
 513 monstrates that employing a multi-modal atten-
 514 tion mechanism to infuse these content features sub-
 515 stantially enhances the subject-fidelity of the gen-
 516 erated samples, yielding a significant increase in the CLIP-I metric.
 517

518 **519 Qualitative analysis of the effect of se-
 520 mantic and content feature injection.** We fur-
 521 ther qualitatively dissect the effect
 522 of each feature component to validate our
 523 design. As shown in Figure 6, starting
 524 from the base Infinity backbone, intro-
 525 ducing semantic features extracted by DI-
 526 NOv2 enables the generator to synthesize
 527 subjects that faithfully preserve the refer-
 528 ence subject’s structure and style. More-
 529 over, further incorporating content fea-
 530 tures from the FLUX.1-dev VAE signif-
 531 icantly enhances EchoGen’s capability to
 532 render fine-grained, coherent details (e.g.,
 533 the facial features of the robot toy and the
 534 fluffy dog, as well as the material and color
 535 of the shoe uppers). These qualitative
 536 results confirm the effectiveness of our dual-
 537 path injection design, where semantic and
 538 content features play distinct yet comple-
 539 mentary roles.
 540

540 6 CONCLUSION

541 This paper presents EchoGen, a novel framework for efficient, feed-forward subject-driven image
 542 synthesis based on a visual autoregressive paradigm, aiming to inherit the properties of high-quality
 543 generation and fast inference speed. Central to our methodology is a dual-path injection me-
 544 chanism, meticulously designed to integrate both the semantic attributes and the precise textural details
 545 of reference images. Comprehensive evaluations corroborate the superiority of our design, revealing
 546 that EchoGen achieves generative performance on par with leading diffusion models while exhib-
 547 iting substantially lower sampling latency. By pioneering a feed-forward, autoregressive solution
 548 for subject-driven synthesis, this research charts a new trajectory for the future development and
 549 application of visual autoregressive generative models.
 550

Module	DINO \uparrow	CLIP-I \uparrow	CLIP-T \uparrow
MM-Attn	0.646	0.792	0.325
Cross-Attn	0.670	0.798	0.322

Table 6: **Different methods for incorporating semantic features.**

Exp.	DINO \uparrow	CLIP-I \uparrow	CLIP-T \uparrow
baseline	0.670	0.798	0.322
+Cross-Attn	0.667	0.803	0.318
+MM-Attn	0.672	0.806	0.321

Table 7: **Impact of injecting subject details.**

504 Considering the absence of lo-
 505 cal details in the semantic features of the refer-
 506 ence images, we incorporate a secondary path-
 507 way that injects localized content features of
 508 the subject. These features, extracted by the
 509 FLUX.1-dev VAE, are used to guide the synthe-
 510 sis of the fine-grained local details of the sub-
 511 ject. The ablation study detailed in Table 7 de-
 512 monstrates that employing a multi-modal atten-
 513 tion mechanism to infuse these content features sub-
 514 stantially enhances the subject-fidelity of the gen-
 515 erated samples, yielding a significant increase in the CLIP-I metric.
 516



Figure 6: **Qualitative analysis of the effect of semantic and content feature injection.**

540 REFERENCES
541

542 Josh Achiam, Steven Adler, Sandhini Agarwal, Lama Ahmad, Ilge Akkaya, Florencia Leoni Ale-
543 man, Diogo Almeida, Janko Altenschmidt, Sam Altman, Shyamal Anadkat, et al. Gpt-4 technical
544 report. *arXiv preprint arXiv:2303.08774*, 2023.

545 Shuai Bai, Keqin Chen, Xuejing Liu, Jialin Wang, Wenbin Ge, Sibo Song, Kai Dang, Peng Wang,
546 Shijie Wang, Jun Tang, Humen Zhong, Yuanzhi Zhu, Mingkun Yang, Zhaohai Li, Jianqiang Wan,
547 Pengfei Wang, Wei Ding, Zheren Fu, Yiheng Xu, Jiabo Ye, Xi Zhang, Tianbao Xie, Zesen Cheng,
548 Hang Zhang, Zhibo Yang, Haiyang Xu, and Junyang Lin. Qwen2.5-v1 technical report. *arXiv*
549 *preprint arXiv:2502.13923*, 2025.

550 Stephen Batifol, Andreas Blattmann, Frederic Boesel, Saksham Consul, Cyril Diagne, Tim Dock-
551 horn, Jack English, Zion English, Patrick Esser, Sumith Kulal, et al. Flux. 1 kontext: Flow match-
552 ing for in-context image generation and editing in latent space. *arXiv e-prints*, pp. arXiv–2506,
553 2025.

554 Huiwen Chang, Han Zhang, Jarred Barber, Aaron Maschinot, Jose Lezama, Lu Jiang, Ming-Hsuan
555 Yang, Kevin Patrick Murphy, William T Freeman, Michael Rubinstein, et al. Muse: Text-to-
556 image generation via masked generative transformers. In *International Conference on Machine*
557 *Learning*, pp. 4055–4075. PMLR, 2023.

558 Wenhui Chen, Hexiang Hu, Chitwan Saharia, and William W. Cohen. Re-imagen: Retrieval-
559 augmented text-to-image generator. In *The Eleventh International Conference on Learning Rep-
560 resentations*, 2023. URL <https://openreview.net/forum?id=XSEBx0iSjFQ>.

561 Jiwoo Chung, Sangeek Hyun, Hyunjun Kim, Eunseo Koh, MinKyu Lee, and Jae-Pil Heo.
562 Fine-tuning visual autoregressive models for subject-driven generation. *arXiv preprint*
563 *arXiv:2504.02612*, 2025.

564 Patrick Esser, Robin Rombach, and Bjorn Ommer. Taming transformers for high-resolution image
565 synthesis. In *Proceedings of the IEEE/CVF conference on computer vision and pattern recogni-
566 tion*, pp. 12873–12883, 2021.

567 Patrick Esser, Sumith Kulal, Andreas Blattmann, Rahim Entezari, Jonas Müller, Harry Saini, Yam
568 Levi, Dominik Lorenz, Axel Sauer, Frederic Boesel, et al. Scaling rectified flow transformers
569 for high-resolution image synthesis. In *Forty-first international conference on machine learning*,
2024.

570 Lijie Fan, Tianhong Li, Siyang Qin, Yuanzhen Li, Chen Sun, Michael Rubinstein, Deqing Sun,
571 Kaiming He, and Yonglong Tian. Fluid: Scaling autoregressive text-to-image generative models
572 with continuous tokens. In *The Thirteenth International Conference on Learning Representations*,
573 2025. URL <https://openreview.net/forum?id=jQP5o1VAvc>.

574 Rinon Gal, Yuval Alaluf, Yuval Atzmon, Or Patashnik, Amit H Bermano, Gal Chechik, and Daniel
575 Cohen-Or. An image is worth one word: Personalizing text-to-image generation using textual
576 inversion. *arXiv preprint arXiv:2208.01618*, 2022.

577 Jian Han, Jinlai Liu, Yi Jiang, Bin Yan, Yuqi Zhang, Zehuan Yuan, Bingyue Peng, and Xiaob-
578 ing Liu. Infinity: Scaling bitwise autoregressive modeling for high-resolution image synthesis.
579 In *Proceedings of the Computer Vision and Pattern Recognition Conference*, pp. 15733–15744,
580 2025.

581 Jonathan Ho and Tim Salimans. Classifier-free diffusion guidance. In *NeurIPS 2021 Workshop on*
582 *Deep Generative Models and Downstream Applications*, 2021. URL <https://openreview.net/forum?id=qw8AKxfYbI>.

583 Jonathan Ho, Ajay Jain, and Pieter Abbeel. Denoising diffusion probabilistic models. *Advances in*
584 *neural information processing systems*, 33:6840–6851, 2020.

585 Edward J Hu, Yelong Shen, Phillip Wallis, Zeyuan Allen-Zhu, Yuanzhi Li, Shean Wang, Lu Wang,
586 Weizhu Chen, et al. Lora: Low-rank adaptation of large language models. *ICLR*, 1(2):3, 2022.

594 Nupur Kumari, Bingliang Zhang, Richard Zhang, Eli Shechtman, and Jun-Yan Zhu. Multi-concept
 595 customization of text-to-image diffusion. In *Proceedings of the IEEE/CVF conference on com-*
 596 *puter vision and pattern recognition*, pp. 1931–1941, 2023.

597

598 Dongxu Li, Junnan Li, and Steven Hoi. Blip-diffusion: Pre-trained subject representation for con-
 599 trollable text-to-image generation and editing. *Advances in Neural Information Processing Sys-*
 600 *tems*, 36:30146–30166, 2023.

601

602 Tianhong Li, Yonglong Tian, He Li, Mingyang Deng, and Kaiming He. Autoregressive image
 603 generation without vector quantization. *Advances in Neural Information Processing Systems*, 37:
 56424–56445, 2024a.

604

605 Xiang Li, Kai Qiu, Hao Chen, Jason Kuen, Zhe Lin, Rita Singh, and Bhiksha Raj. Controlvar:
 606 Exploring controllable visual autoregressive modeling. *arXiv preprint arXiv:2406.09750*, 2024b.

607

608 Zongming Li, Tianheng Cheng, Shoufa Chen, Peize Sun, Haocheng Shen, Longjin Ran, Xiaoxin
 609 Chen, Wenyu Liu, and Xinggang Wang. Controlar: Controllable image generation with autore-
 610 gressive models. In *International Conference on Learning Representations*, 2025.

611

612 Shilong Liu, Zhaoyang Zeng, Tianhe Ren, Feng Li, Hao Zhang, Jie Yang, Qing Jiang, Chunyuan
 613 Li, Jianwei Yang, Hang Su, et al. Grounding dino: Marrying dino with grounded pre-training
 614 for open-set object detection. In *European conference on computer vision*, pp. 38–55. Springer,
 2024.

615

616 Ilya Loshchilov and Frank Hutter. Decoupled weight decay regularization. *arXiv preprint*
 617 *arXiv:1711.05101*, 2017.

618

619 Jian Ma, Junhao Liang, Chen Chen, and Haonan Lu. Subject-diffusion: Open domain personalized
 620 text-to-image generation without test-time fine-tuning. In *ACM SIGGRAPH 2024 Conference*
 621 *Papers*, pp. 1–12, 2024.

622

623 Fabian Mentzer, David Minnen, Eirikur Agustsson, and Michael Tschannen. Finite scalar quantiza-
 624 tion: VQ-VAE made simple. In *The Twelfth International Conference on Learning Representa-*
 625 *tions*, 2024. URL <https://openreview.net/forum?id=8ishA3LxN8>.

626

627 Maxime Oquab, Timothée Darcet, Théo Moutakanni, Huy V. Vo, Marc Szafraniec, Vasil Khali-
 628 dov, Pierre Fernandez, Daniel HAZIZA, Francisco Massa, Alaaeldin El-Nouby, Mido Assran,
 629 Nicolas Ballas, Wojciech Galuba, Russell Howes, Po-Yao Huang, Shang-Wen Li, Ishan Misra,
 630 Michael Rabbat, Vasu Sharma, Gabriel Synnaeve, Hu Xu, Herve Jegou, Julien Mairal, Patrick
 631 Labatut, Armand Joulin, and Piotr Bojanowski. DINOv2: Learning robust visual features with-
 632 out supervision. *Transactions on Machine Learning Research*, 2024. ISSN 2835-8856. URL
 633 <https://openreview.net/forum?id=a68SUt6zFt>. Featured Certification.

634

635 Xichen Pan, Li Dong, Shaohan Huang, Zhiliang Peng, Wenhui Chen, and Furu Wei. Kosmos-g:
 636 Generating images in context with multimodal large language models. In *The Twelfth Interna-*
 637 *tional Conference on Learning Representations*, 2024. URL <https://openreview.net/foru>
 638 *id=he6mX9LTyE*.

639

640 Maitreya Patel, Sangmin Jung, Chitta Baral, and Yezhou Yang. λ -ECLIPSE: Multi-concept per-
 641 sonalized text-to-image diffusion models by leveraging CLIP latent space. *Transactions on Machine*
 642 *Learning Research*, 2024. ISSN 2835-8856. URL <https://openreview.net/foru>
 643 *id=7q5Uew1AdM*.

644

645 Yuang Peng, Yuxin Cui, Haomiao Tang, Zekun Qi, Runpei Dong, Jing Bai, Chunrui Han, Zheng Ge,
 646 Xiangyu Zhang, and Shu-Tao Xia. Dreambench++: A human-aligned benchmark for personalized
 647 image generation. *arXiv preprint arXiv:2406.16855*, 2024.

648

649 Dustin Podell, Zion English, Kyle Lacey, Andreas Blattmann, Tim Dockhorn, Jonas Müller, Joe
 650 Penna, and Robin Rombach. SDXL: Improving latent diffusion models for high-resolution image
 651 synthesis. In *The Twelfth International Conference on Learning Representations*, 2024. URL
 652 <https://openreview.net/foru>*id=di52zR8xgf*.

648 Senthil Purushwarkam, Akash Gokul, Shafiq Joty, and Nikhil Naik. Bootpig: Bootstrapping zero-
 649 shot personalized image generation capabilities in pretrained diffusion models. In *European Con-*
 650 *ference on Computer Vision*, pp. 252–269. Springer, 2024.

651 Alec Radford, Karthik Narasimhan, Tim Salimans, Ilya Sutskever, et al. Improving language under-
 652 standing by generative pre-training. 2018.

653 Alec Radford, Jong Wook Kim, Chris Hallacy, Aditya Ramesh, Gabriel Goh, Sandhini Agarwal,
 654 Girish Sastry, Amanda Askell, Pamela Mishkin, Jack Clark, et al. Learning transferable visual
 655 models from natural language supervision. In *International conference on machine learning*, pp.
 656 8748–8763. PMLR, 2021.

657 Aditya Ramesh, Mikhail Pavlov, Gabriel Goh, Scott Gray, Chelsea Voss, Alec Radford, Mark Chen,
 658 and Ilya Sutskever. Zero-shot text-to-image generation. In *International conference on machine*
 659 *learning*, pp. 8821–8831. Pmlr, 2021.

660 Robin Rombach, Andreas Blattmann, Dominik Lorenz, Patrick Esser, and Björn Ommer. High-
 661 resolution image synthesis with latent diffusion models. In *Proceedings of the IEEE/CVF confer-*
 662 *ence on computer vision and pattern recognition*, pp. 10684–10695, 2022.

663 Nataniel Ruiz, Yuanzhen Li, Varun Jampani, Yael Pritch, Michael Rubinstein, and Kfir Aberman.
 664 Dreambooth: Fine tuning text-to-image diffusion models for subject-driven generation. In *Pro-*
 665 *ceedings of the IEEE/CVF conference on computer vision and pattern recognition*, pp. 22500–
 666 22510, 2023.

667 Chitwan Saharia, William Chan, Saurabh Saxena, Lala Li, Jay Whang, Emily L Denton, Kamyar
 668 Ghasemipour, Raphael Gontijo Lopes, Burcu Karagol Ayan, Tim Salimans, et al. Photorealistic
 669 text-to-image diffusion models with deep language understanding. *Advances in neural informa-*
 670 *tion processing systems*, 35:36479–36494, 2022.

671 Tim Salimans, Andrej Karpathy, Xi Chen, and Diederik P. Kingma. PixelCNN++: Improving the
 672 pixelCNN with discretized logistic mixture likelihood and other modifications. In *International*
 673 *Conference on Learning Representations*, 2017. URL <https://openreview.net/forum?id=BJrFC6ceg>.

674 Chaehun Shin, Jooyoung Choi, Heeseung Kim, and Sungroh Yoon. Large-scale text-to-image model
 675 with inpainting is a zero-shot subject-driven image generator. In *Proceedings of the Computer*
 676 *Vision and Pattern Recognition Conference*, pp. 7986–7996, 2025.

677 Lingchen Sun, Rongyuan Wu, Zhiyuan Ma, Shuaizheng Liu, Qiaosi Yi, and Lei Zhang. Pixel-
 678 level and semantic-level adjustable super-resolution: A dual-lora approach. In *Proceedings of the*
 679 *Computer Vision and Pattern Recognition Conference*, pp. 2333–2343, 2025.

680 Peize Sun, Yi Jiang, Shoufa Chen, Shilong Zhang, Bingyue Peng, Ping Luo, and Zehuan Yuan.
 681 Autoregressive model beats diffusion: Llama for scalable image generation. *arXiv preprint*
 682 *arXiv:2406.06525*, 2024.

683 Zhenxiong Tan, Songhua Liu, Xingyi Yang, Qiaochu Xue, and Xinchao Wang. Ominicontrol: Mini-
 684 mal and universal control for diffusion transformer. In *Proceedings of the IEEE/CVF International*
 685 *Conference on Computer Vision*, 2025.

686 Keyu Tian, Yi Jiang, Zehuan Yuan, Bingyue Peng, and Liwei Wang. Visual autoregressive modeling:
 687 Scalable image generation via next-scale prediction. *Advances in neural information processing*
 688 *systems*, 37:84839–84865, 2024.

689 Michael Tschannen, Alexey Gritsenko, Xiao Wang, Muhammad Ferjad Naeem, Ibrahim Alabdul-
 690 mohsin, Nikhil Parthasarathy, Talfan Evans, Lucas Beyer, Ye Xia, Basil Mustafa, et al. Siglip 2:
 691 Multilingual vision-language encoders with improved semantic understanding, localization, and
 692 dense features. *arXiv preprint arXiv:2502.14786*, 2025.

693 Aaron Van den Oord, Nal Kalchbrenner, Lasse Espeholt, Oriol Vinyals, Alex Graves, et al. Con-
 694 ditional image generation with pixelcnn decoders. *Advances in neural information processing*
 695 *systems*, 29, 2016.

702 Xierui Wang, Siming Fu, Qihan Huang, Wanggui He, and Hao Jiang. MS-diffusion: Multi-subject
 703 zero-shot image personalization with layout guidance. In *The Thirteenth International Conference on Learning Representations*, 2025. URL <https://openreview.net/forum?id=PJqP0wyQek>.

704

705

706 Yuxiang Wei, Yabo Zhang, Zhilong Ji, Jinfeng Bai, Lei Zhang, and Wangmeng Zuo. Elite: Encoding
 707 visual concepts into textual embeddings for customized text-to-image generation. In *Proceedings of the IEEE/CVF International Conference on Computer Vision*, pp. 15943–15953, 2023.

708

709

710 Chengyue Wu, Xiaokang Chen, Zhiyu Wu, Yiyang Ma, Xingchao Liu, Zizheng Pan, Wen Liu,
 711 Zhenda Xie, Xingkai Yu, Chong Ruan, et al. Janus: Decoupling visual encoding for unified
 712 multimodal understanding and generation. *arXiv preprint arXiv:2410.13848*, 2024.

713

714 Shaojin Wu, Mengqi Huang, Wenxu Wu, Yufeng Cheng, Fei Ding, and Qian He. Less-to-
 715 more generalization: Unlocking more controllability by in-context generation. *arXiv preprint arXiv:2504.02160*, 2025.

716

717 Shitao Xiao, Yueze Wang, Junjie Zhou, Huaying Yuan, Xingrun Xing, Ruiran Yan, Chaofan Li,
 718 Shuting Wang, Tiejun Huang, and Zheng Liu. Omnigen: Unified image generation. In *Proceedings of the Computer Vision and Pattern Recognition Conference*, pp. 13294–13304, 2025.

719

720 Ziyu Yao, Jialin Li, Yifeng Zhou, Yong Liu, Xi Jiang, Chengjie Wang, Feng Zheng, Yuexian Zou,
 721 and Lei Li. Car: Controllable autoregressive modeling for visual generation. *arXiv preprint arXiv:2410.04671*, 2024.

722

723 Hu Ye, Jun Zhang, Sibo Liu, Xiao Han, and Wei Yang. Ip-adapter: Text compatible image prompt
 724 adapter for text-to-image diffusion models. *arXiv preprint arXiv:2308.06721*, 2023.

725

726 Jiahui Yu, Xin Li, Jing Yu Koh, Han Zhang, Ruoming Pang, James Qin, Alexander Ku, Yuanzhong
 727 Xu, Jason Baldridge, and Yonghui Wu. Vector-quantized image modeling with improved
 728 VQGAN. In *International Conference on Learning Representations*, 2022a. URL <https://openreview.net/forum?id=pfNyExj7z2>.

729

730 Jiahui Yu, Yuanzhong Xu, Jing Yu Koh, Thang Luong, Gunjan Baid, Zirui Wang, Vijay Vasudevan,
 731 Alexander Ku, Yinfei Yang, Burcu Karagol Ayan, Ben Hutchinson, Wei Han, Zarana Parekh, Xin
 732 Li, Han Zhang, Jason Baldridge, and Yonghui Wu. Scaling autoregressive models for content-rich
 733 text-to-image generation. *Transactions on Machine Learning Research*, 2022b. ISSN 2835-8856.
 734 URL <https://openreview.net/forum?id=AFDcYJKhND>. Featured Certification.

735

736 Yu Zeng, Vishal M Patel, Haochen Wang, Xun Huang, Ting-Chun Wang, Ming-Yu Liu, and Yogesh
 737 Balaji. Jedi: Joint-image diffusion models for finetuning-free personalized text-to-image genera-
 738 tion. In *Proceedings of the IEEE/CVF Conference on Computer Vision and Pattern Recognition*,
 739 pp. 6786–6795, 2024.

740

741 Hao Zhang, Feng Li, Shilong Liu, Lei Zhang, Hang Su, Jun Zhu, Lionel M Ni, and Heung-Yeung
 742 Shum. Dino: Detr with improved denoising anchor boxes for end-to-end object detection. *arXiv
 743 preprint arXiv:2203.03605*, 2022.

744

745 Lvmin Zhang, Anyi Rao, and Maneesh Agrawala. Adding conditional control to text-to-image
 746 diffusion models. In *Proceedings of the IEEE/CVF international conference on computer vision*,
 747 pp. 3836–3847, 2023.

748

749 Yuxuan Zhang, Yirui Yuan, Yiren Song, Haofan Wang, and Jiaming Liu. Easycontrol: Adding
 750 efficient and flexible control for diffusion transformer. *arXiv preprint arXiv:2503.07027*, 2025.

751

752

753

754

755

756 7 APPENDIX
757758 7.1 DATASET
759

760 Following common practices like **OminiControl** (Tan et al., 2025) and **EasyControl** (Zhang et al.,
761 we train EchoGen on the synthetic Subjects200K dataset. The Subjects200K dataset¹, in-
762 introduced by (Tan et al., 2025), comprises approximately 256,000 data triplets, each consisting of a
763 reference image, a textual prompt, and a corresponding generated sample. This dataset was specif-
764 ically established for subject-driven generative tasks. The curation process began by leveraging
765 ChatGPT-4o to generate over 30,000 diverse subject descriptions, each description portraying the
766 same subject across multiple scenes. Subsequently, these descriptions were reformulated into struc-
767 tured prompts, each detailing a single subject in two distinct scenes. These prompts were then used
768 as input for the FLUX.1-dev model to synthesize image pairs. In the final stage, GPT-4o was em-
769 ployed to filter the resulting pairs, validating both subject consistency and overall image quality. All
770 images within the dataset feature a resolution exceeding 500 pixels, ensuring sufficient detail for
771 model training.

772 7.2 PSEUDO-CODE OF THE ECHOGEN BLOCK
773

774 We provide a PyTorch-style pseudocode for our EchoGen Block in Algorithm 1 to facilitate repro-
775 ducibility and clarity.

777 7.3 IMPLEMENTATION DETAILS
778

779 7.3.1 TRAINING DETAILS

780 **Data Preprocessing.** All training images undergo a standardized pre-processing pipeline. Initially,
781 images are resized so that their shorter edge matches the model’s target resolution, which is 256
782 pixels for EchoGen-0.1B and 1024 pixels for EchoGen-2B, followed by a central crop to achieve a
783 square aspect ratio.

784 To maintain data quality for high-resolution image generation within the EchoGen-2B model, we
785 circumvent the quality degradation induced by naive bilinear upsampling. Instead of using simple
786 bilinear scaling on images smaller than 1024 pixels, we integrate a super-resolution step. Specifi-
787 cally, we leverage the PiSA-SR model (Sun et al., 2025) to upscale these images, a method chosen to
788 preserve fine-grained textures and prevent the introduction of common interpolation artifacts. This
789 ensures that the model is trained exclusively on high-quality and high-resolution exemplars.

790 **Training Hyper-parameters.** We follow the Infinity-2B standard training recipe (Han et al., 2025),
791 and the detailed hyperparameter configurations used to train our EchoGen are provided in Table 8.
792 To mitigate error accumulation, as mentioned in Infinity, we employ bitwise self-correction by ran-
793 domly flipping bits in the input sequence with a probability of 0.3. To improve robustness against
794 variations in instruction length, prompts are randomly truncated to a single sentence with a probabili-
795 ty of 0.5 during training. The EchoGen models are trained using 32 H20 GPUs, requiring 2 weeks
796 for the longest schedule (training our EchoGen-2B model for 20 epochs).

798 7.3.2 EVALUATION DETAILS
799

800 For our quantitative evaluation, we utilize the DreamBench dataset (Ruiz et al., 2023). The dataset
801 comprises 30 distinct subjects, categorized into 9 animate pets (cats and dogs) and 21 diverse inani-
802 mate objects (e.g., toys, sunglasses, backpacks). Each subject is associated with 25 textual prompts
803 specifically designed to test the model’s abilities in recontextualization, property modification, and
804 accessorization. Our data preparation protocol is adapted from (Pan et al., 2024), which involves
805 selecting a single reference image per subject and augmenting its subject identity phrase with de-
806 scriptive keywords. The correspondence between the DreamBench dataset directory name and the
807 augmented subject description is summarized as follows:

808 • backpack, backpack
809

¹<https://huggingface.co/datasets/Yuanshi/Subjects200K>

```

810  class EchoGenBlock(nn.Module):
811      def __init__(self, dim, mask):
812          # Multi-modal attention QKV projectors for the image token sequence
813          self.qkv_mm = nn.Linear(dim, 3*dim)
814          # Multi-modal attention QKV projectors for the detailed content feature
815          self.qkv_mm_c = nn.Linear(dim, 3*dim)
816          self.mask = mask
817
818          # Cross attention query projectors for the image token sequence
819          self.q_ca = nn.Linear(dim, dim)
820          # Cross attention KV projectors for the semantic feature
821          self.kv_ca_s = nn.Linear(dim, 2*dim)
822          # Cross attention KV projectors for the text embedding
823          self.kv_ca_t = nn.Linear(dim, 2*dim)
824
825          # FFN for the image token sequence
826          self.ffn = MLP(dim)
827          # FFN for the detailed content feature
828          self.ffn_c = MLP(dim)
829
830      def forward(self, x, cc, cs, ct):
831          # Multi-modal attention
832          q, k, v = self.qkv_mm(x)
833          qc, kc, vc = self.qkv_mm(cc)
834
835          q = torch.concat((q, qc))
836          k = torch.concat((k, kc))
837          v = torch.concat((v, vc))
838          x, cc = attention(q, k, v, self.mask)
839
840          # Cross attention
841          q = self.q_ca(x)
842          ks, vs = self.kv_ca_s(cs)
843          kt, vt = self.kv_ca_t(ct)
844
845          k = torch.concat((ks, kt))
846          v = torch.concat((vs, vt))
847          x = attention(q, k, v, mask=None)
848
849          # Feed-forward network
850          x = self.ffn(x)
851          cc = self.ffn_c(cc)
852
853      return x, cc, cs, ct

```

Pseudo-code illustrating the EchoGen Block. Here, x denotes the image token sequence, and the generation process is conditioned on the semantic feature c_s and detailed content feature c_c extracted from the reference image, along with the text embedding c_t .

- backpack_dog, dog shaped backpack
- bear_plushie, bear plushie
- can, 'Transatlantic IPA' can
- candle, jar candle
- cat, tabby cat
- cat2, grey cat
- clock, number '3' clock
- colorful_sneaker, colorful sneaker
- dog1, fluffy dog
- dog2, fluffy dog
- dog3, curly-haired dog
- dog5, long-haired dog
- dog6, puppy
- dog7, dog
- dog8, dog
- duck_toy, duck toy

Config	value
Bitwise Self-correction Flip Ratio	0.3
Bitwise Self-correction Apply Layers	13
Dynamic Truncate Prompt Ratio	0.5
Infinity Image Encoder Channel	16(0.1B) / 32(2B)
Text Encoder	Flan-t5-xl
Text Embedding Channels	2048
Maximum Text Tokens Length	512
Semantic Image Encoder	DINO-v2-Base
Semantic Feature Channels	768
Semantic Downsample ratio	14
Content Image Encoder	FLUX.1-dev VAE
Content Feature Channels	16
Content Downsample ratio	8
Reweighting Loss by Scale	True
Gradient clipping by norm	5.0
Optimizer	Adamw
Beta1	0.9
Beta2	0.97
Decay	0
Base Learning rate	3e-5
Multi-Modal Modules Learning rate	3e-6
Learning rate warmup iterations	0
Training epochs	20
Total Batchsize	128
GPU	H20

Table 8: **Detailed hyper-parameters for training our EchoGen.**

- fancy_boot, fringed cream boot
- grey_sloth_plushie, grey sloth plushie
- monster_toy, monster toy
- pink_sunglasses, sunglasses
- poop_emoji, poop-emoji shaped toy
- rc_car, car toy
- red_cartoon, cartoon character
- robot_toy, robot toy
- shiny_sneaker, sneaker
- teapot, clay teapot
- vase, tall vase
- wolf_plushie, wolf plushie

To augment the diversity and rigor of our human evaluation, we incorporate a curated set of instances from the DreamBench++ benchmark. DreamBench++ includes 150 subjects, each paired with nine prompts.

7.4 MORE ABLATION STUDIES

In this section, we present additional ablation studies to analyze the individual components of EchoGen. These ablation studies are also conducted based on EchoGen-0.1B model with fair training settings.

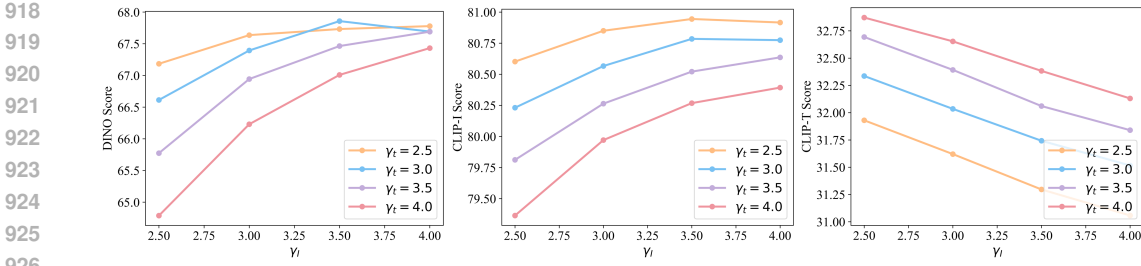


Figure 7: Visualization of the effect of classifier-free guidance scale coefficient.

Importance of injecting global semantic information. Injecting global semantic information serves as a prepended condition, to ensure global structural coherence during generation. Our ablation study in Table 5 confirms the significant benefits of incorporating global semantic features. Moreover, we conduct a targeted experiment comparing the injection of global semantic versus content features to the Image Token. As shown in Table 9, the results clearly indicate that prepending semantic features rather than content information into the image token significantly enhances the subject fidelity. This confirms that our choice to inject global semantic guidance into image tokens is both effective and well-justified.

Subject Segmentation. To mitigate the influence of irrelevant background noise and focus on the primary subject, we leverage the Qwen2.5-VL vision language model (Bai et al., 2025) and the GroundingDINO segmentation from the reference image. We conducted an ablation study, detailed in Table 10, to validate the efficacy of the echo segmentation protocol. The results confirm that the introduction of subject segmentation significantly enhances the generation performance, which is observed in the preservation of subject features, and demonstrate that isolating the main subject is critical to producing more accurate and faithful outputs.

To further analyze the sensitivity of our method to the quality of segmentation, we conduct an ablation study on about EchoGen’s robustness to segmentation quality during inference. Specifically, to simulate segmentation imperfections, we design three variants to simulate disturbances and compare with employing subject segmentation without imperfection during inference: 1. Enlarging Bounding Box: enlarging the subject’s bounding box by 10%; 2. Shifting Bounding Box: shifting the bounding box by 10%; 3. No Segmentation: completely removing the subject segmentation step. As shown in Table 11, our model exhibits remarkable robustness as its performance degrades only slightly under these disturbances. Moreover, our model still produces strong results even without any segmentation, demonstrating its powerful generalization capability. In summary, EchoGen is highly robust to imperfect segmentation.

Exp.	DINO↑	CLIP-I↑	CLIP-T↑
Content	0.663	0.795	0.322
Semantic	0.672	0.806	0.321

Table 9: Analysis of different information types prepended to the Image Token. Content represents prepending the global content feature, while Semantic denotes prepending the global semantic feature.

Exp.	DINO↑	CLIP-I↑	CLIP-T↑
w/o SS	0.663	0.796	0.321
w/ SS	0.672	0.806	0.321

Table 10: Enhancement by subject segmentation (denoted by SS) to mitigate background noise.

Exp.	DINO↑	CLIP-I↑	CLIP-T↑
w/o SS	0.737	0.829	0.324
Shift	0.739	0.833	0.321
Enlarge	0.735	0.831	0.321
w/ SS	0.755	0.837	0.324

Table 11: Analysis of the sensitivity of our method to the quality of the segmentation. SS denotes the subject segmentation; Enlarge and Shift denote enlarging and shifting bounding box, respectively.

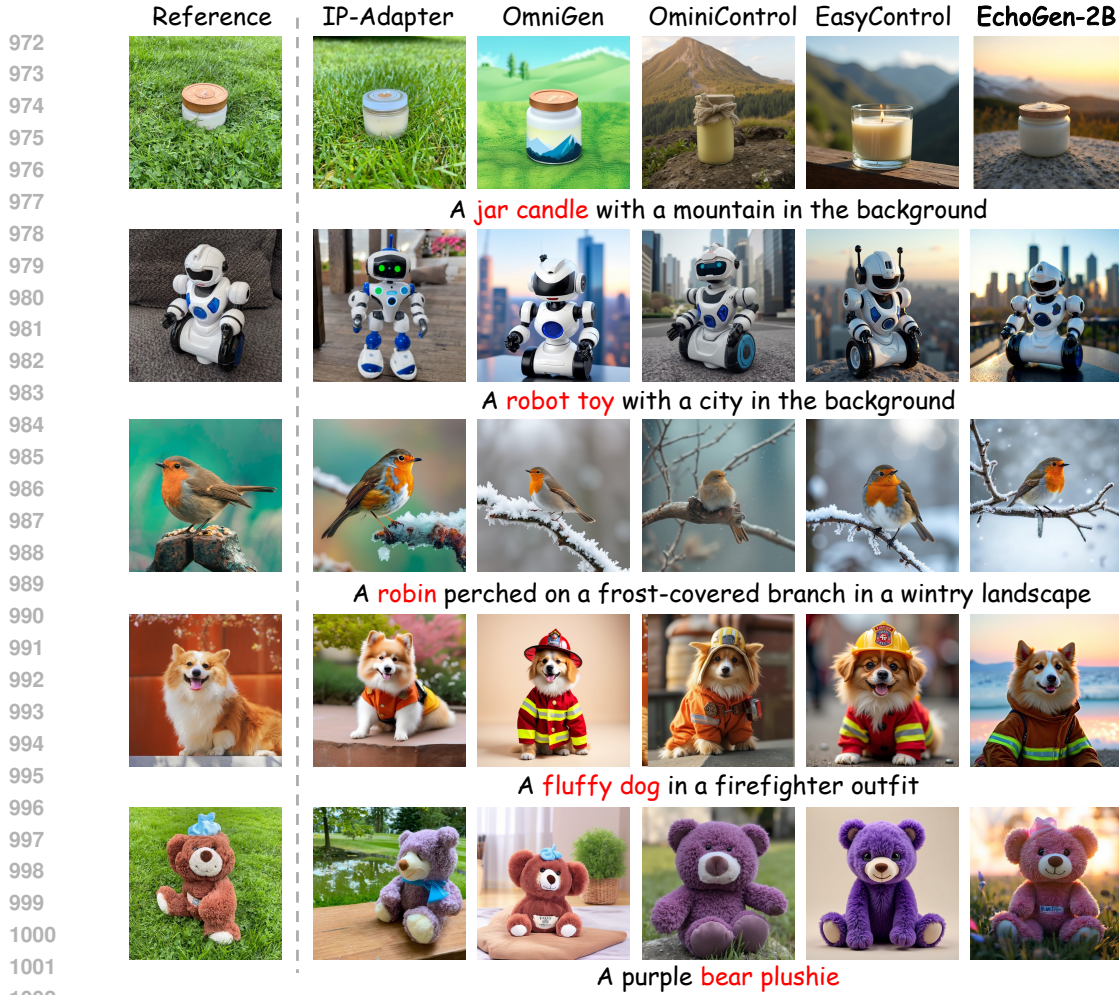


Figure 8: Additional qualitative comparisons between our EchoGen model and competing methods.

Subject-text classifier-free guidance. As detailed in Figure 7, our experiments reveal a clear trade-off governed by the CFG hyperparameters within a proper scope. As the subject guidance weight γ_I increases, subject fidelity improves, as indicated by higher CLIP-I and DINO scores. Conversely, this gain is accompanied by reduced text alignment, reflected in lower CLIP-T. The inverse relationship is observed when increasing the text condition scaling coefficient γ_t . This empirical result demonstrates the efficacy and flexibility of our CFG design, enabling users to dynamically adjust the balance between preserving reference image features and adhering to the text prompt.

7.5 MORE VISUALIZATION RESULTS

We further showcase additional qualitative results on DreamBench in Figure 8. Moreover, we provide additional visual results from the EchoGen-2B model on real-world subject personalization in Figure 9. These results demonstrate that, with training exclusively on the large-scale high-quality synthetic dataset Subjects200K, our model exhibits strong generalization to real-world scenarios, including the generation of live animals and diverse objects under complex conditions. EchoGen-2B consistently maintains high subject fidelity and strong text alignment during these real-world

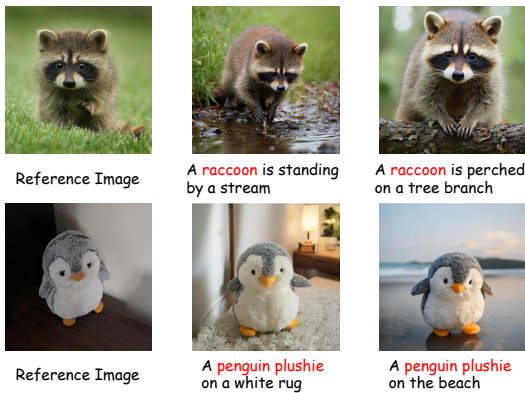


Figure 9: More visualization of EchoGen-2B on real-world subject personalization.



Figure 10: Failure cases generated by EchoGen.

personalization tasks, demonstrating the effectiveness of our training strategy and the proposed dual-path semantic-content injection design.

7.6 LIMITATION & FAILURE CASE ANALYSIS

Our EchoGen takes a new step toward VAR-based feed-forward subject-driven generation to inherit the strong capability of next-scale prediction and bidirectional modeling within scales. However, we know that the feed-forward subject-driven image generation is highly dependent on the capability of base models. The performance of our EchoGen models is fundamentally dependent upon the capability of the base models Infinity-0.1B and Infinity-2B. The Infinity-2B architecture still exhibits a performance gap compared to state-of-the-art generation models such as Stable-Diffusion 3 and FLUX, particularly in generating high-fidelity details. This inherited constraint limits EchoGen’s efficacy in resolving fine-grained features, such as the faithful rendering of facial characteristics, the synthesis of coherent text, and the reproduction of intricate material textures. Due to significant GPU computational and temporal constraints, our experiments are confined to these specific backbones, precluding an empirical investigation of larger models such as Infinity-8B. We hypothesize that migrating the EchoGen architecture to a more potent VAR foundation model would unlock substantial performance gains.

Additionally, the DINOv2 vision encoder operates on relatively low-resolution inputs (e.g., 224×224), which limits its ability to capture fine-grained appearance cues and tiny textual elements. We believe seeking an effective high-resolution semantic encoder presents a promising avenue for further improvement in complex applications.

Due to the aforementioned limitations, as illustrated in Figure 10, the model exhibits reduced reliability on subjects that have highly intricate structures or in scenarios requiring precise text rendering. We will continue to investigate and address these challenges in future work.

7.7 THE USAGE OF LARGE LANGUAGE MODEL

We utilized the large language models Qwen-3 and GPT-5 to improve the clarity, grammar, and formal tone of the writing in the method and experiment sections. Nevertheless, all technical content, such as conceptual formulas and experiments remain our own; the large language models were used solely as tools for linguistic enhancement and stylistic polishing.